

# Accuracy of Displacement Estimation and Selection of Capacitors for a Four Degrees of Freedom Capacitive Force Sensor

Chisato Murakami and Makoto Takahashi

**Abstract**—Force sensor has been used as requisite for knowing information on the amount and the directions of forces on the skin surface. We have developed a four-degrees-of-freedom capacitive force sensor (approximately  $20 \times 20 \times 5$  mm<sup>3</sup>) that has a flexible structure and sixteen parallel plate capacitors. An iterative algorithm was developed for estimating four displacements from the sixteen capacitances using fourth-order polynomial approximation of characteristics between capacitance and displacement. The estimation results from measured capacitances had large error caused by deterioration of the characteristics. In this study, effective capacitors had major information were selected on the basis of the capacitance change range and the characteristic shape. Maximum errors in calibration and non-calibration points were 25% and 6.8%. However the maximum error was larger than desired value, the smallness of averaged value indicated the occurrence of a few large error points. On the other hand, error in non-calibration point was within desired value.

**Keywords**—Force sensors, capacitive sensors, estimation, iterative algorithms.

## I. INTRODUCTION

IT has been reported that major factor leading to the development of pressure ulcers is force generated at the skin surface. Information on the amount and the directions of forces is important for prevention of pressure ulcers such as the setup of force dispersion from the skin surface [1]. Devices for measuring forces on the skin interface have been used for risk evaluation of ulcers and development of effective mattress and cushion [2]. These sensors have thin and flexible structure and the ability to measure pressure and shear forces in single or multipoint [3], [4].

To obtain more information on the amount and the directions of forces, we have developed a four-degrees-of-freedom (DOF) capacitive force sensor [5] that has a flexible structure and four upper and lower electrodes for which combinations function as sixteen capacitors (Fig. 1). For estimating forces, it is necessary to estimate displacements of directions of four DOF forces from sixteen capacitances as measuring value of the sensor. Capacitance curve for each displacement component had nonlinearity in all capacitors and quadratic function type in some capacitors because of the structure and measuring range

of the sensor. For estimating outputs of the nonlinear sensor, efficient means have been reported in the area of analog and digital processing including linearization technique [6]–[9]. In recent study, estimation using artificial neural network (ANN), which have the ability of superior nonlinear approximation, were achieved in good accuracy in conditions of nonlinear sensor response affected by environmental parameters of temperature and humidity [10], [11]. However, it is difficult to track the calculation process of ANNs. There, we had developed an iterative algorithm for solving the four DOF displacements from sixteen measured capacitances using fourth-order polynomial approximation of sensor characteristics, which represented the relationship between displacements and capacitances. The solution search by iterative method is standard technique and has been used in numerical analysis. In our algorithm, estimating displacement component is selected from among four DOF displacements in each iterative count and the estimating value is calculated from approximate functions. The deficient component of displacement is detected by search table and residual values between measuring and estimating capacitances. Maximum deficient component corresponds to an estimating displacement in next iterative count. Search table shows changing capacitance trend for complex displacement of four DOF components. The default values of approximation coefficient and search table are arranged by calibration data in advance. The accuracy was good in simulation by theoretical capacitances [12]. Compared with theoretical curves, estimated displacements from measured capacitances had large error rate because measured sensor characteristics had small values. It is difficult to be estimating component the displacement had decreasing of capacitance change. Error rate of the displacement component is large by the effect. To improve the error, two search tables derived from calibration data by theoretical equation were used for displacement estimation from measuring capacitances. One table was the same as the search table used in estimation of theoretical data and the other was a table that had high sensitivity in the displacement had small capacitance change. In this result, maximum error for full scale (FS) displacement range was less than 18%. However, the method using two tables by theoretical data is impractical for further improvements of accuracy in the condition of capacitance curves that varied between theoretical and measured data.

There, we focused on a selection of important measuring data for displacement estimation. Some capacitance

C. Murakami is with the Graduate School of Information Science and Technology, Hokkaido University, Sapporo 060-0814, Japan (e-mail: Murakami\_Chisato@ist.hokudai.ac.jp).

M. Takahashi is with the Graduate School of Information Science, Hokkaido University, Sapporo 060-0814, Japan (e-mail: Takahashi\_Makoto@ist.hokudai.ac.jp).

characteristics of sixteen capacitors for each displacement have nonlinearity and non-monotonicity as quadratic function types. To remove ambiguity of information in quadratic characteristics, capacitance data of capacitors that had monotonic characteristics were used to search deficient displacement in each repetition. In this study, we reported selection of capacitors and accuracy of displacement estimation using measured capacitance values.

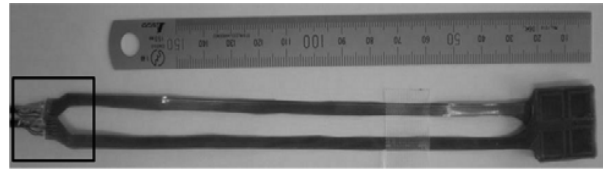


Fig. 4 The fabricated sensor. The square of left side is the connection between electrode lines and four-core shielded cable

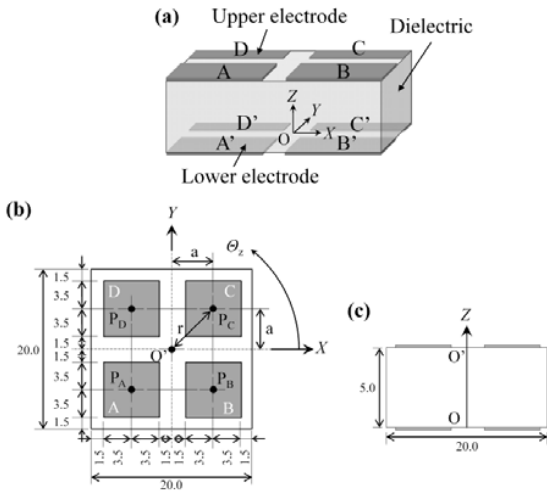


Fig. 1 The structure and the coordinate system of the developed sensor. (a) The overall view (b) The top view (c) The side view

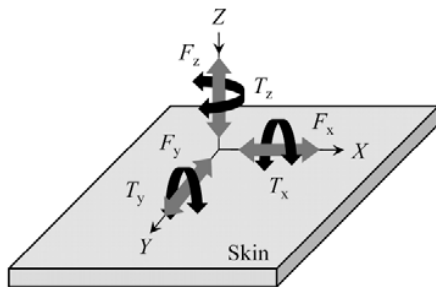


Fig. 2 Four DOF displacements and forces. Four DOF displacements are defined as  $X, Y, Z, \theta_z$  and four DOF forces are defined as  $F_x, F_y, F_z, T_z$ .

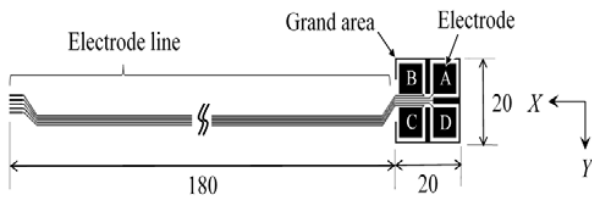


Fig. 3 The electrode pattern of electrodes and electrode lines on FPCB (unit: mm). The electrode lines derived each electrode are connected to measurement instrument

II. SENSOR THEORY

Shear, normal and yaw forces  $F_x, F_y, F_z$  and  $T_z$  forces in the directions of  $X, Y$  and  $Z$  and  $\theta_z$  were defined as shown in Fig. 2. The sensor was constructed from a cubic dielectric (silicone gel,  $20 \times 20 \times 5 \text{ mm}^3$ ) and two substrates (flexible printed circuit board (FPCB), approximately  $20 \times 20 \text{ mm}^2$ ). The electrodes (copper,  $7 \times 7 \text{ mm}^2$ ) were arranged in four per substrate. We named the upper electrodes A, B, C, and D and the lower electrodes A', B', C', and D' as shown in Fig. 1. There is a total of sixteen combinations of upper and lower electrodes, AA', AB', ..., DC', DD', which were denoted by  $i = 1, 2, \dots, 15, 16$ , respectively. Each paired electrode has the function of a parallel plate capacitor. The desired displacement range (full scale) was defined as  $-2.0$  to  $2.0$  (4.0) mm in  $X$  and  $Y$ ,  $0$  to  $2.0$  (2.0) mm in  $Z$  and  $-10$  to  $10$  (20) deg in  $\theta_z$ .

In theory, the capacitance value  $C_i$  in a parallel plate capacitor  $i$  is defined as (1).

$$C_i = \epsilon_0 \epsilon_r S / D_i, \tag{1}$$

where  $\epsilon_0$  is the permittivity of vacuum,  $\epsilon_r$  is the relative permittivity of the dielectric material (4.8),  $S$  is the area of the parallel plate electrode, and  $D_i$  is the distance between the center points of the upper and lower electrodes.

The electrode pattern of the substrate was formulated as shown in Fig. 3. The substrate was constructed from four electrodes, ground area, and five lines. Four lines were connected to each electrode and one line was connected to the ground area. The pattern was exposed on FPCB (Sunhayato, 1K, Japan). Then the substrate was formed by etching. Fig. 4 shows the fabricated sensor. The gel and two substrates were bonded with double-sided tape that had silicone and acrylic pressure-sensitive adhesiveness and a thickness of 0.085 mm. The lines on the substrates were connected to a four-core shielded cable for reduction of power noise (approximately 300 mm) in a square of Fig. 4.

The silicone gel was selected as a dielectric material for measuring skin surface force. The selected gel had 50% of strain when the standard pressure, which was skin surface pressure of 200 mmHg (about 0.0266 MPa) in seated position, was applied to the sensor.

The normal and shear strains  $\epsilon, \gamma_x$  and  $\gamma_y$  calculated from the displacements  $Z, X$  and  $Y$  were used for force estimation. The normal and shear stresses  $\sigma, \tau_x$  and  $\tau_y$  can be calculated by Hooke's law using the normal and shear strains and are denoted as (2).

$$\begin{aligned}\sigma &= E\varepsilon, \\ \tau_x &= G\gamma_x, \\ \tau_y &= G\gamma_y,\end{aligned}\quad (2)$$

where  $E$  is the compressive elastic modulus and  $G$  is the modulus of rigidity.  $E$  was defined as a constant value of 54.1 kPa in 25% strain of the gel. The normal, shear and yaw forces  $F_z$ ,  $F_x$ ,  $F_y$  and  $T_z$  applied to the sensor were calculated in (3).

$$\begin{aligned}F_z &= \sigma A, \\ F_x &= \tau_x A, \\ F_y &= \tau_y A, \\ T_z &= GI_p \Theta_z / l,\end{aligned}\quad (3)$$

where  $A$  is the cross-sectional area of the pressure direction,  $l$  is the length of the sensor in the pressure axis under an unloaded condition and  $I_p$  is the second moment in a rectangular section [5]. The forces at a single point are read out in real time.

### III. ESTIMATION ALGORITHM

#### A. Objective Function

Equation (4) was objective function of the iterative calculation for detecting four displacements from sixteen capacitances.

$$R_i = f(x_1) - y_i, \quad (4)$$

where  $y_i$  corresponds to capacitance  $C_i$ ,  $f(x_1)$  is the approximate capacitance calculated by an approximate function,  $x_1$  is estimated displacement, and  $R_i$  is residual error in a capacitor  $i$ .  $x_1$  is determined by solving the objective function as a minimization problem of  $R_i$ . A component of four displacements is estimated in one count of iteration. The capacitance characteristics are approximated by a fourth-order polynomial. The coefficient of determination was more than 0.9 in all characteristics. Approximate function  $f(x_1)$  is defined as (5).

$$f(x_1) = \sum_{k_1=0}^4 a_{k_1 i} x_1^{k_1}, \quad (5)$$

where  $a_i$  is the approximation coefficient and  $x_1$  is estimated displacement of one component in an iteration count  $n$ . Coefficient  $a_i$  has a nested structure and was calculated in the fourth-order polynomial as (6).

$$\begin{aligned}a_{k_1 i} &= \sum_{k_2=0}^4 b_{k_1 k_2 i} x_2^{k_2}, \\ b_{k_1 k_2 i} &= \sum_{k_3=0}^4 c_{k_1 k_2 k_3 i} x_3^{k_3}, \\ c_{k_1 k_2 k_3 i} &= \sum_{k_4=0}^4 d_{k_1 k_2 k_3 k_4 i} x_4^{k_4},\end{aligned}\quad (6)$$

where  $b_i, c_i$  and  $d_i$  are approximation coefficients and  $d_i$  is a constant value, which is obtained from calibration data.  $x_2, x_3$ , and  $x_4$  are three other DOF displacements except for  $x_1$  and default values of those are zero.  $a_i, b_i$ , and  $c_i$  are calculated by substitution of  $x_2, x_3, x_4$  for (6).  $x_2, x_3$ , and  $x_4$  are updated by the estimated displacements until the current count of iteration. Four displacements handle  $x_1$  in turns in each repetition. Calibration data are capacitances in 625 displacement conditions consisting of combinations of five calibration points for each displacement (Table I).

#### B. Algorithm

The algorithm was developed in MATLAB. The flow of the estimation algorithm (Fig. 5) is as follows:

- 1) Substitute capacitances  $C_i$  into input values  $y_i$ .
- 2) Set and update parameters in  $n$ .
- 3) Calculate approximation coefficients  $c_i, b_i, a_i$  and solutions  $x_{1i}$ .
- 4) Determine estimated displacement  $x_1$ .
- 5) Update displacements in  $n$ .
- 6) Calculate estimated capacitances  $f(x_1(n))$  and residual errors  $R_i$ .
- 7) Determine search displacement and direction.
- 8) Test for convergence.

Firstly, capacitances measured by measuring circuit are substituted for  $y_i$  in process 1). Iteration starts from process 2). Default values are set to the parameters in  $n = 1$ . Default values of the constraint condition were defined as  $-2.5$  to  $2.5$  mm in  $X$  and  $Y$ ,  $0$  to  $2.5$  mm in  $Z$  and  $-15$  to  $15$  deg in  $\Theta_z$ . Estimated displacement in the last count is updated every count of  $n > 1$  to the maximum or minimum value of the constraint condition. Default values of displacements  $x_2, x_3, x_4$  were zero. Updating parameters, which are displacement  $x_2, x_3, x_4$  estimated until  $n-1$  and constraint condition are set in  $n > 1$ . In process 3), coefficients  $a_i, b_i, c_i$  in (5) and (6) are calculated by substitution of  $d_i, x_2, x_3$ , and  $x_4$ . Solutions  $x_{1i}$  are calculated by (7).

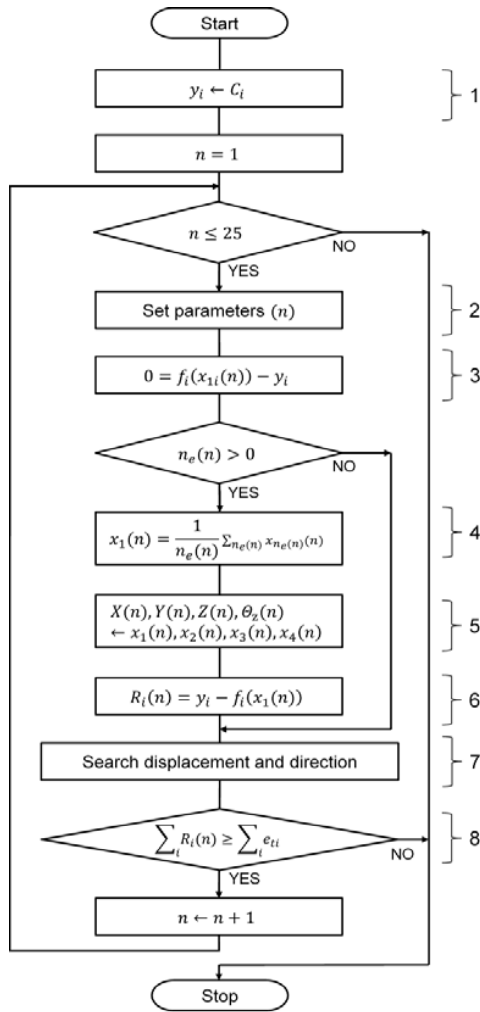


Fig. 5 Flow chart of the algorithm

$$0 = f(x_{1i}(n)) - y_i. \tag{7}$$

Because  $x_{1i}$  have four solutions including real and imaginary numbers in each  $i$ , the real root is selected in the range of constraint condition as effective solution. If estimated values are close to optimum values,  $x_1$  has similar values in all capacitors. An estimated value  $x_1$  is an average value of the number of the effective solution  $n_e$  in process 4). If effective solution is nothing, come back to process 2) and  $Z$  is estimating displacement in  $n + 1$ . Estimated and substituted displacements  $x_1, x_2, x_3,$  and  $x_4$  are stored in estimated displacement matrix  $X(n), Y(n), Z(n),$  and  $\Theta_z(n)$ , respectively(process 5)). In process 6), estimated capacitances  $f(x_1(n))$  are calculated by substitution of determined single value  $x_1$ . Residual errors  $R_i$  are calculated by (4). In process 7), component of search displacement and direction, which indicates estimating displacement component  $x_1$  in  $n + 1$ , is

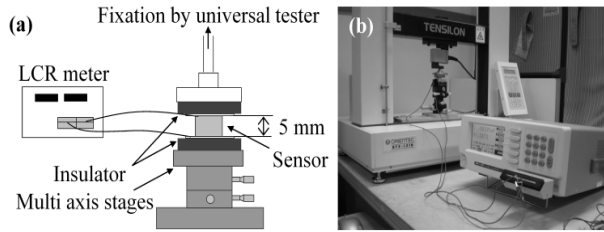


Fig. 6 Experimental system (a) Image of the system (b) Photograph of capacitance measurement

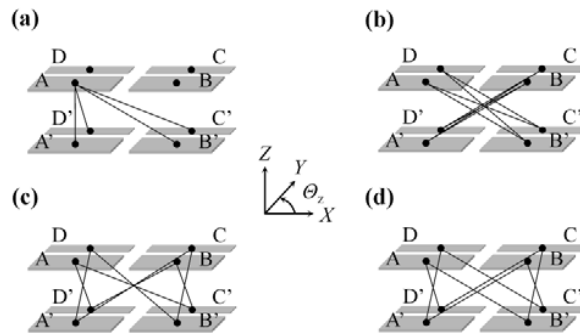


Fig. 7 Effective capacitors in each displacement component Default distance between electrodes of capacitor AC' ( $i = 3$ ) in unloaded condition is the longer in capacitors had upper electrode of A. (a). The effective capacitors had monotonicity curve are different for displacement  $X$  (b), displacement  $Y$  (c), and displacement  $\Theta_z$  (d)

selected from eight patterns:  $X+, X-, Y+, Y-, Z+, Z-, \Theta_z+$ , and  $\Theta_z-$  (+: increasing, -: decreasing). Two decision points, residual and estimated number points, are used for determining deficient component and priority of estimating displacement. A deficient displacement component in  $n$  is detected by comparison between the trends of residual errors  $R_i$  and the search table, which is developed from calibration data. The search table shows the increasing and decreasing trends of capacitance change in all capacitors for displacement change. Residual point is degree of coincidence between codes of binarized residual error and binarized search table in each pattern. Meanwhile, estimated number point results from estimated number in each displacement until  $n$ . Probability density function of  $\chi^2$  distribution (two degrees of freedom) is

TABLE I  
DISPLACEMENT CONDITION FOR CALIBRATION

| Direction        | Displacement Condition |     |     |     |    |
|------------------|------------------------|-----|-----|-----|----|
|                  | 1                      | 2   | 3   | 4   | 5  |
| $X$ (mm)         | -2                     | -1  | 0   | 1   | 2  |
| $Y$ (mm)         | -2                     | -1  | 0   | 1   | 2  |
| $Z$ (mm)         | 0.5                    | 0.8 | 1.2 | 1.6 | 2  |
| $\Theta_z$ (deg) | -10                    | -5  | 0   | 5   | 10 |

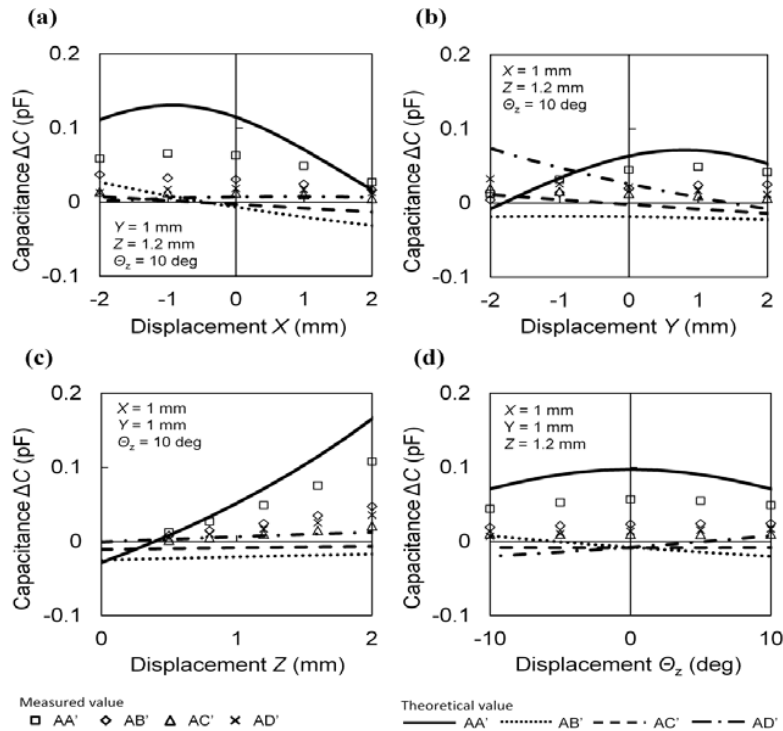


Fig. 8 Theoretical and measured capacitance changes for each displacement in capacitors of developed sensor. Capacitance  $\Delta C$  is difference value in loaded and unloaded conditions for displacements  $X$  (a),  $Y$  (b),  $Z$  (c), and  $\Theta_z$  (d)

used for expression of estimated number. The displacement component  $Z^+$  is estimated in the first count  $n=1$  because  $Z$  has positive value under any circumstance of displacements. The same component is not selected as  $x_1$  continuously between counts because  $x_2, x_3, x_4$  are not updated. Search component is determined in the sum of residual and estimated number points. In process 8), if  $R_i$  in all capacitors are sufficiently small values, the iteration is stopped. The sum of absolute norms of  $R_i$  is used

for the convergence criterion. The iteration is discontinued when the sum of  $R_i$  is less than sum of 0.5% capacitances ( $e_{vi}$ ) in the loaded condition of  $X=0$  mm,  $Y=0$  mm,  $Z=2$  mm and  $\Theta_z=0$  deg. The sixteen capacitances of the threshold value are maximum values in the measuring range of the sensor. After completing process 8), the processes from process 2) are repeated set number of repetition.

TABLE II  
DISPLACEMENT CONDITION FOR NON-CALIBRATION

| Direction        | Displacement Condition |     |     |     |     |     |     |     |     |     |
|------------------|------------------------|-----|-----|-----|-----|-----|-----|-----|-----|-----|
|                  | 1                      | 2   | 3   | 4   | 5   | 6   | 7   | 8   | 9   | 10  |
| $X$ (mm)         | 1.5                    | 1.5 | 1.5 | 1.5 | 1.5 | 1.5 | 1.5 | 1.5 | 1.5 | 1.5 |
| $Y$ (mm)         | 1.5                    | 1.5 | 1.5 | 1.5 | 1.5 | 1.5 | 1.5 | 1.5 | 1.5 | 1.5 |
| $Z$ (mm)         | 0.2                    | 0.4 | 0.6 | 0.8 | 1.0 | 1.2 | 1.4 | 1.6 | 1.8 | 2   |
| $\Theta_z$ (deg) | 8                      | 8   | 8   | 8   | 8   | 8   | 8   | 8   | 8   | 8   |

#### IV. METHOD

##### A. Theoretical Capacitance

Theoretical capacitance was calculated by (1). Theoretical  $D_i$  was defined as (8) from the displacement conditions.

$$\begin{aligned}
 D_i &= \sqrt{D_{xi}^2 + D_{yi}^2 + D_{zi}^2}, \\
 D_x &= r \cos \varphi - (X + r \cos \varphi'), \\
 D_y &= r \sin \varphi - (Y + r \sin \varphi'), \\
 D_z &= 5 - Z, \\
 \varphi' &= \varphi + \Theta_z,
 \end{aligned} \tag{8}$$

where  $r$  was the distance between the origin  $O$  and the center point of the lower electrode and was a constant value of 7.07 mm (Fig. 1 (b)).  $\varphi$  was the initial position angle of the center point of the upper electrode  $P_A, P_B, P_C,$  and  $P_D$  in an unloaded condition. The initial angles of the upper and lower electrodes in an unloaded condition were  $\varphi_A = \varphi_{A'} = 45$  deg,  $\varphi_B = \varphi_{B'} = 135$  deg,  $\varphi_C = \varphi_{C'} = 225$  deg, and  $\varphi_D = \varphi_{D'} = 315$  deg.  $\varphi'$  was the position angle of the center point of the lower electrode  $P_{A'}, P_{B'}, P_{C'},$  and  $P_{D}'$  in a loaded condition.

### B. Experimental Setup

The capacitance was measured using an experimental system (Fig. 6). The system was constructed from multi-axis stages (XYZ $\theta\alpha\beta$  axis stages, SIGMA KOKI, Japan), an LCR meter (KC-567, KOKUYO ELECTRIC, Japan), and a universal tester (TENSILON, RTE-1210, ORIENTEC, Japan). The measurement conditions were voltage source of AC1V, measuring frequency of 100 kHz and measurement time of 896 ms in a measuring point. Displacements instead of forces were applied to the lower surface of the sensor by the multi-axis stages. Displacement conditions of measuring points were as shown in Table I and Table II. The displacement conditions in calibration and non-calibration points were 625 (Table I) and 10 (Table II) points. The capacitance values of sixteen capacitors were measured by the LCR meter. Capacitances in unloaded and loaded conditions were measured in a displacement condition only once. Repeatability of measurement was confirmed in [5]. The difference between capacitances of two conditions was used for estimation as capacitance change.

### C. Selection of Effective Capacitor

Measured curves of sensor characteristics had nonlinearly and non-monotonicity. Especially, capacitance change curves for displacements  $X$ ,  $Y$  and  $\theta_z$  had non-monotonicity as quadratic function type in some capacitors. Maximal or minimal of the curves of quadratic function type moved to positive or negative direction of the displacement by the composition of displacement components of  $X$ ,  $Y$  and  $\theta_z$  and the position gap between upper and lower substrates when assembling the sensor. Search table, which is binary data, cannot conform to the moving. -And, capacitance change was small in a capacitor that had long default distance between upper and lower electrodes. For example, the longest default

distance was AC' in capacitors had upper electrode of A as shown in Fig. 7 (a). There, we considered information from the capacitors, which had the characteristics of quadratic function type and small capacitance change, as inferior quality. However, information of the capacitors was also excluded from the information used in comparison of residual errors and search table. We selected effective capacitors in each displacement component for decreasing redundancy and noise contained in measuring data. Effective capacitors had sensor characteristics of monotonic curves were AB', AC', BA', BD', CA', CD', DB', DC' ( $i = 2, 3, 5, 8, 9, 12, 14, 15$ ) in  $X$  (Fig. 7 (b)), AC', AD', BC', BD', CA', CB', DA', DB' ( $i = 3, 4, 7, 8, 9, 10, 13, 14$ ) in  $Y$  (Fig. 7 (c)),  $i = 1, 6, 11, 16$  in  $Z$  and AB', AD', BA', BC', CB', CD', DA', DC' ( $i = 2, 4, 5, 7, 10, 12, 13, 15$ ) in  $\theta_z$  (Fig. 7 (d)). The effective capacitors were used in comparison of residual error and search table for obtaining residual point in each estimation of displacement components except estimation of  $Z$ . Information of all capacitors was used to obtain residual point in the estimation of  $Z$  because of reduction of the error factor by occurrence of pitch and roll forces  $T_x, T_y$ .

### D. Set Parameters and Evaluation Index

After completing process 8) of the algorithm, the process 2) is repeated 60 times. Updating value of constraint condition was returned to default value when approximate function had no effective solution in  $n \geq 40$ . The probability density function was multiplied by 80 as gain.

The accuracy of estimation was evaluated using measured data in calibration and non-calibration points. The approximation coefficient  $d_i$  and search table were created by measured calibration data. The evaluation index was full scale error (FSE). Absolute errors for 1% FSE corresponded to 0.04 mm in  $X$  and  $Y$ , 0.02 mm in  $Z$ , and 0.2 deg in  $\theta_z$ .

TABLE III  
FULL SCALE ERROR FOR CALIBRATION AND NON-CALIBRATION POINTS

| Direction        | %FSE in calibration point |         | %FSE in non-calibration point |         |
|------------------|---------------------------|---------|-------------------------------|---------|
|                  | Maximum                   | Average | Maximum                       | Average |
| $X$ (mm)         | 25                        | 2.9     | 6.8                           | 3.2     |
| $Y$ (mm)         | 12                        | 1.2     | 2.2                           | 0.97    |
| $Z$ (mm)         | 12                        | 1.4     | 4.3                           | 2.3     |
| $\theta_z$ (deg) | 21                        | 2.7     | 6.5                           | 1.9     |

TABLE IV  
FULL SCALE ERROR FOR NON-CALIBRATION POINTS

| Direction        | Displacement Condition |      |       |        |     |     |     |     |      |      |
|------------------|------------------------|------|-------|--------|-----|-----|-----|-----|------|------|
|                  | 1                      | 2    | 3     | 4      | 5   | 6   | 7   | 8   | 9    | 10   |
| $X$ (mm)         | 3.5                    | 0.92 | 3.5   | 5.2    | 3.1 | 2.8 | 6.8 | 4.1 | 1.0  | 0.67 |
| $Y$ (mm)         | 0.0087                 | 2.2  | 0.036 | 0.0067 | 2.0 | 1.5 | 1.3 | 1.1 | 0.76 | 0.72 |
| $Z$ (mm)         | 0.27                   | 0.25 | 0.53  | 3.8    | 3.9 | 3.1 | 4.3 | 3.1 | 2.1  | 1.5  |
| $\theta_z$ (deg) | 1.7                    | 2.7  | 0.28  | 0.29   | 1.3 | 2.9 | 6.5 | 1.5 | 1.3  | 0.10 |

## V. RESULTS AND DISCUSSION

### A. Sensor Characteristic

Fig. 8 shows theoretical capacitance change calculated by (1) and measured capacitance change in calibration data for each

displacement in the capacitors of AA', AB', AC', AD' ( $i = 1, 2, 3, 4$ ). Parameters of three other DOF displacements were  $Y = 1$  mm,  $Z = 1.2$  mm,  $\theta_z = 10$  deg in Fig. 8 (a),  $X = 1$  mm,  $Z = 1.2$  mm,  $\theta_z = 10$  deg in Fig. 8 (b),  $X = 1$  mm,  $Y = 1$  mm,  $\theta_z = 10$  deg in Fig. 8 (c), and  $X = 1$  mm,  $Y = 1$  mm,  $Z = 1.2$  mm in Fig. 8 (d).

Capacitance changes of vertical axis were difference values between capacitances in loaded and unloaded displacement conditions. Measured values were small values compared with theoretical values in whole. It was considered that the difference occurred by the pattern of electrode lines, weakness of insulating in the measurement, and position gap between upper and lower electrodes in assembling of the sensor.

#### B. Accuracy of Estimation

Table III shows FSE values in calibration points of 625 and non-calibration points of 10. In the results of calibration points, maximum FSE in 625 points was 25% in  $X$  direction and the error value was larger than desired error value of less than 20%. The estimating value of  $X$  converged on a value around a true value in estimated number of 45 in the estimation. However, output value of  $X$  was different from the convergence value because final estimating value was obtained in estimating displacement in a count had minimum sum value of residual errors of all capacitors. Averaged FSE of  $X$  direction in 625 points was 2.9% and had good accuracy. The averaged value indicated the few large FSE points. The estimation error might be able to be improved by detection of similarity in conditions of the large FSE. The right side of Table III and Table IV shows FSE values in non-calibration points. Maximum FSE in 10 points was 6.8% and it was within the desired error value. It is necessary for evaluation to increase the number of measuring points in non-calibration points.

In the estimation using two search tables, time requirements for estimations by calibration and non-calibration data were approximately 15.6 min and 1.1 min, respectively [12]. On the other hand, time requirements in calibration and non-calibration data were approximately 78 min and 1.6 min in Table III and Table IV. Calculation time of a measuring point was approximately 7.5 sec to 9.6 sec. Increase of time requirements in calibration points indicated to fail to pass the test for convergence in most measuring points. In actuality, measuring time is determined from start of capacitance measurement to output of estimated forces. Even if optimization is performed in the algorithm, it requires further improvement.

Error rates are the same in displacement estimation and force estimation because we assume that the elastic modulus of silicone gel is constant in force estimation. Actually, however, force varies nonlinearly with strain by change of elastic modulus. Therefore, estimated force has error factor in the force estimation method. It may be possible to use same algorithm in force estimation for solving the error by change of elastic modulus.

## VI. CONCLUSION

We have developed a four-DOF capacitive force sensor for measuring forces on the skin and it has a flexible structure and sixteen capacitors. The capacitance characteristics for each displacement had nonlinearity and non-monotonicity. We developed iterative method using approximate function by fourth order polynomial as nonlinear capacitance characteristics for estimating four displacements from sixteen

capacitances. In this study, we selected important information from capacitors and the iterative method was evaluated using the information. In the estimated four DOF displacements, error values for sensor full scale were less than 25% in calibration points and 6.8% in non-calibration points. The averaged error values were good in many estimation points.

In actuality, estimated force has error factor by change of elastic modulus. It may be possible to use same algorithm in force estimation for solving error by change of elastic modulus. We have developed processing circuit for capacitance measurement by AD7746 (Analog devices, USA).

## REFERENCES

- [1] M. Baharestani, et al., "International Review: Pressure ulcer prevention: pressure, shear, friction and microclimate in context," *L. MacGregor.Ed. London: Wounds International*, 2010.
- [2] D. M. Brienza, P. E. Karg, M. J. Geyer, S. Kelsey, and E. Trefler, "The relationship between pressure ulcer incidence and buttock-seat cushion interface pressure in at-risk elderly wheelchair users," *Archives of physical medicine and rehabilitation*, vol. 82, pp. 529-33, Apr. 2001.
- [3] T. Ohura, M. Takahashi, and N. Ohura, "Influence of external forces (pressure and shear force) on superficial layer and subcutis of porcine skin and effects of dressing materials: are dressing materials beneficial for reducing pressure and shear force in tissues?," *Wound repair and regeneration*, vol. 16, pp. 102-7, Jan-Feb. 2008.
- [4] S. Baron and G. MacFarlane, "Reducing pressure ulcer risk in the operating room," *Hill-Rom Company White Paper 2009*.
- [5] C. Murakami, Y. Ishikuro, and M. Takahashi, "Feasibility of novel four degrees of freedom capacitive force sensor for skin interface force," *Biomedical engineering online*, 11:90, Nov. 2012.
- [6] P. P. L. Regtien and P. J. Trimp, "Dynamic calibration of sensors using EEPROMs," *Sensors and Actuators A: Physical*, vol. 22, pp. 615-618, 1989.
- [7] K. F. Lyahou, G. van der Horn, and J. H. Huijsing, "A noniterative polynomial 2-D calibration method implemented in a microcontroller," *IEEE Transactions on Instrumentation and Measurement*, vol. 46, pp. 752-757, Aug. 1997.
- [8] P. Hille, R. Höhler, and H. Strack, "A linearisation and compensation method for integrated sensors," *Sensors and Actuators A: Physical*, vol. 44, pp. 95-102, Aug. 1994.
- [9] G. Bucci, M. Faccio, and C. Landi, "New ADC with piecewise linear characteristic: case study-implementation of a smart humidity sensor," *IEEE Transactions on Instrumentation and Measurement*, vol. 49, pp. 1154-1166, 2000.
- [10] S. Aoyagi, M. Kawanishi, and D. Yoshikawa, "Multiaxis Capacitive Force Sensor and its Measurement Principle Using Neural Networks," *Journal of Robotics and Mechatronics*, vol. 18, no. 4, pp. 442-449, 2006.
- [11] J. C. Patra, E. L. Ang, A. Das, and N. S. Chaudhari, "Auto-compensation of nonlinear influence of environmental parameters on the sensor characteristics using neural networks," *ISA transactions*, vol. 44, pp. 165-76, Apr. 2005.
- [12] C. Murakami and M. Takahashi, "Evaluation of iterative algorithm performance in a four degrees of freedom capacitive force sensor on the skin interface," unpublished.